Journal of Multiscale Modelling

World Scientific
www.worldscientific.com

A MULTISCALE APPROACH TO FAILURE ASSESSMENT IN DEPLOYMENT FOR CARDIOVASCULAR STENTS

F. HAREWOOD[*,†], J. GROGAN[*] and P. Mc HUGH[*,†]

[*]*Department of Mechanical and Biomedical Engineering,*
National University of Ireland, Galway,
University Road, Galway, Ireland

[†]*National Centre for Biomedical Engineering and Science,*
National University of Ireland, Galway,
University Road, Galway, Ireland

Cardiovascular stents are tiny scaffolds that are used in the treatment of heart disease. The recent development of drug-eluting stents has lead to stent implantation in arterial regions that would previously have been considered too complex. Deployment in these tortuous and branched regions results in an increased deformation of the stent. It is thus important to assess whether there is an increased likelihood of stent failure in deployment in such regions. A multiscale approach, incorporating the results of microscale modelling of failure in individual stent struts and macroscale modelling of stent deployment in realistic arterial geometries is considered in this work. Such an approach allows for a more accurate assessment of failure than is obtainable through the macroscale modelling of deployment in idealized arterial geometries alone, as is presented in previous studies. Results give an insight into failure risks for different stent implantation scenarios: stent failure is unlikely in deployment in tortuous vessels, however there may be risks associated with certain bifurcational stenting techniques.

Keywords: Explicit finite element; microscale size effects; realistic artery geometry.

1. Introduction

Atherosclerosis is the leading cause of death in the western world.[1] In atherosclerosis, which is a form of heart disease, fatty material in the blood is deposited on the internal surface of the coronary arteries (the arteries that deliver blood to the heart muscle). A sufficient build-up of deposits at a particular location results in a stenosis that can partially or completely block the artery. The stenosis can remain soft (fatty) or can become hard and brittle (calcified). This condition can be treated by angioplasty, where an angioplasty catheter (narrow hollow tube) with a balloon on the distal (leading) end is inserted into the arterial system and tracked to the site of the blockage. The balloon is inflated, expanding the blockage, deflated and removed. The balloon inflation also expands (deploys) a stent (a tubular wire-mesh-like structure) that is mounted on the balloon, and when the balloon is removed the stent remains as a permanent implant to keep the artery open, thereby ensuring adequate blood flow to the heart muscle.

Balloon expandable stents have commonly been made from medical grade 316L austenitic stainless steel and laser cutting the stent pattern from a thin tube is a typical method of manufacture. In terms of dimensions for coronary applications, tubes typically have outside diameters of 1 to 1.5 mm and wall thicknesses of 0.085 to 0.1 mm.

Following laser cutting and other treatments involving annealing and electro-polishing, the stent is crimped onto the balloon catheter. Deploying the stent by balloon expansion results in plastic deformation in the metal which, in turn, ensures that the stent retains a permanently expanded state. A certain level of elastic recoil occurs on deflation and removal of the balloon.

The introduction of Drug-Eluting Stents (DES) has resulted in a significant decrease in the occurrence of restenosis, or post-deployment re-narrowing of the artery lumen.[2] Along with trends in industry to develop stents with thinner struts, this has given clinicians the confidence to deploy stents in arterial regions that would previously have been considered too tortuous or narrow. Deployments of stents in bifurcated, or branched, arteries are also becoming more common, despite considerable distortion of the deployed stents during such procedures. Due to the increased deformation of stents during insertion and deployment in modern procedures, and in light of several reports of *in vivo* stent failure in the literature (e.g. Sianos *et al.*[3] and Takebayashi *et al.*[4]) a method to assess stent failure risk during deployment, that is reflective of the small physical size scale of stents and its direct influence on stent strut mechanical properties, would be extremely useful in the stent design phase.

Computational analysis is an important tool in stent design and is proving an increasingly viable alternative to costly experimental testing.[5,6] By now a wealth of computational studies involving stents is available in the literature. Many such studies have modelled stent deployment in straight, cylindrical arteries.[7,8] However it is important to also account for additional deformation due to deployment in more complex vessel geometries, including arterial bifurcations, such as in the work of Mortier *et al*.[9] In the present work this is accomplished through the use of physiologically realistic artery geometries, based on clinical biplane angiograms of healthy blood vessels as used by O'Keefe *et al.*[10] Further to this, it has been observed experimentally that microscale size effects have a significant influence on the ductility of thin stainless steel struts.[11,12] Despite this, many computational studies involving stents have used material data based on the properties of large scale samples,[13,14] thus over-estimating the ductility of the stent struts. In this study, material data that accounts for the experimentally observed size effect is used. This data is based on the microscale computational modelling work of Savage *et al.*,[15] Murphy *et al.*[12] and, in particular, Harewood and McHugh,[16] who employed a rate-dependent, crystal plasticity model in the simulated multi-mode loading of thin stainless steel struts.

Against this backdrop, this paper presents a size-dependent failure risk assessment methodology for stent deployment. A multiscale approach is taken, involving a combination of microscale and macroscale modelling. Macroscale simulations of deployments of entire stents in realistic artery geometries are first performed. This allows for an evaluation of the local deformation during deployment in individual stent struts and plastic hinges, circled in Fig. 1. An assessment of the likelihood of stent failure can then be made, based on the results of the multi-mode microscale modelling of individual stent struts and hinges, as carried out by Harewood and McHugh.[16] This application of multiscale modelling allows for a more realistic assessment of the likelihood of stent failure than has been achievable in the past.

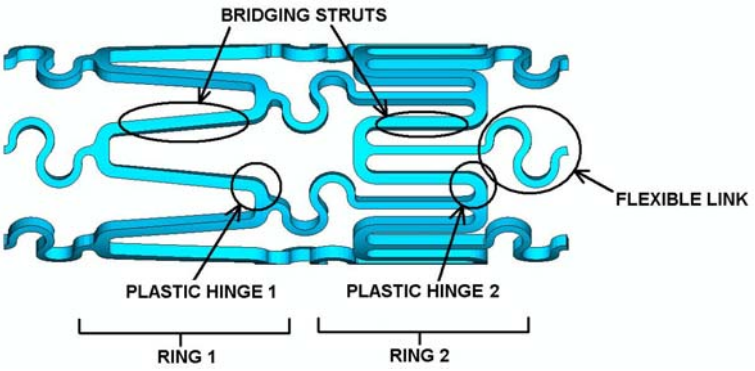

Fig. 1. A section of the generic stent geometry used in this study. Individual struts and plastics hinges are circled.

2. Theory and Model Description

2.1. *Macroscale stent modelling*

Macroscale modelling of stent deployment in realistic arterial geometries is performed in this study. The stent material is chosen as stainless steel 316L, which is considered to be elastic-plastic. The ABAQUS® finite element program is used for the simulations, and finite deformation kinematics is assumed. The material properties are taken from the work of Harewood and McHugh[16] for stainless steel struts of thickness 75 μm. Elasticity is considered to be linear and isotropic in terms of finite deformation quantities, with a Young's Modulus of E = 193 GPa and Poisson's Ration of υ = 0.3. Plasticity is described by isotropic hardening J_2 flow theory, where the specific form of the strain hardening curve is taken from Ref. 16, in terms of a series of data points, including a yield strength of 450 MPa and a UTS of 801 MPa at an engineering plastic strain of 0.22. Fracture is not explicitly modelled at the macroscale.

A generic stent geometry is used in this study (Fig. 2), representative of commercially available stent geometries, and which is based on the BiodivYsio OpenCell commercial stent. Thicknesses of the struts range between 50 and 80 μm, with a constant radial depth of 90 μm. A finite element model of the stent was created using PATRAN® meshing software, based on its unit cell geometry, with the mesh consisting of 64 000 linear brick elements (C3D8R). Linear elements were chosen based on the reasoning that they perform better than second order elements in contact analyses and that the use of second order elements may have lead to convergence issues.[17] Prior to the simulation of deployment, for the different cases described below, the initially straight stent is deformed so that its curvature conforms to the corresponding curved arterial geometries that are used,[10] an example of which is shown in Fig. 3. This pre-deployment curvature is accomplished by fixing one end of the originally straight stent in position and applying a simultaneous displacement and rotation to the other end. This is done in such a manner as to prevent localized deformation of the struts. This process is carried out through use of ABAQUS®/Standard and the resulting deformed mesh is exported for use in subsequent analyses. Deployment of the stent is accomplished through the application of a uniform pressure to its inner surface, an approach that is common in the literature.[7,13] In order to ensure a realistic dog-bone profile in the expanding stent that is similar to that described

by Migliavacca *et al.*,[18] an additional pressure is applied to its ends during deployment.[19] The use of pressure to simulate stent expansion is simpler than the explicit balloon expansion method of Mortier *et al.*[20] and Gervaso *et al.*[21] but is considered justified here for the following reasons: 1) for practicality due to the very large computational problem sizes incorporating stent, artery and arterial surrounds (established through initial mesh sensitivity studies), and the geometrical irregularity and consequent inability to exploit symmetry efficiencies; 2) the focus on the *final* deformed configuration of the stent to make the failure risk assessment rather than the stent deformation evolution during expansion.

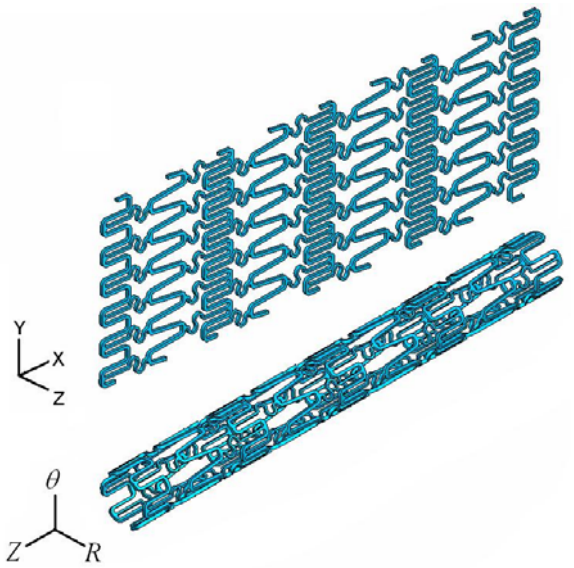

Fig. 2. Planar and cylindrical representation of the undeformed stent geometry used in this work.

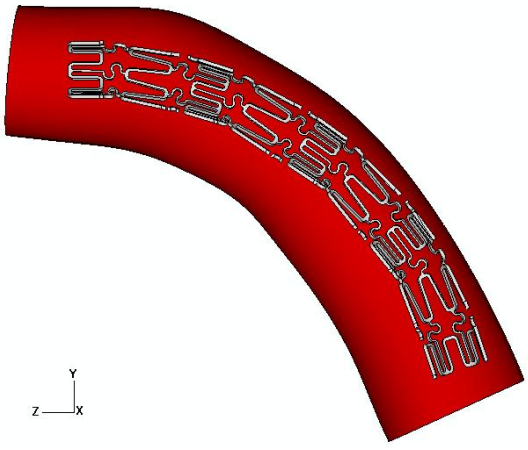

Fig. 3. Section view of the deformed stent geometry in the curved artery geometry.

Realistic geometries of tortuous and bifurcated arteries, based on biplane angiograms of healthy vessels from O'Keefe *et al.*[10] are used in this study. A hyperelastic consituitive model is used to represent the behaviour of the artery wall. A reduced form of the polynomial hyperelastic model, as established by Prendergast *et al.*[22] and based on experimental testing of human artery tissue is employed. The reduced strain energy function *U*, determined by Prendergast *et al.*,[22] is given as:

$$U = C_{10}(\bar{I}_1 - 3) + C_{01}(\bar{I}_2 - 3) + C_{20}(\bar{I}_1 - 3)^2 + C_{11}(\bar{I}_1 - 3)(\bar{I}_2 - 3) + C_{30}(\bar{I}_2 - 3)^3 \quad (1)$$

where C_{ij} are material constants and $\bar{I}_1$ and $\bar{I}_2$ are the respective first and second strain invariants of the left Cauchy-Green strain tensor. Material constants used in the description of the artery wall from Ref. 7 are listed in Table 1.

Table 1. Arterial tissue constants to describe a Mooney-Rivlin hyperelastic model.[7]

Material Properties (kPa)	
C_{10}	18.90
C_{01}	2.75
C_{11}	85.72
C_{20}	590.43
C_{30}	0.00

2.2. *Microscale stent modelling and failure risk assessment*

The failure risk assesment used in this study is based on a multiscale approach, linking the results of the detailed multi-mode microscale simulations of Harewood and McHugh[16] with the results of the macroscale stent delpoyment simulations described in the next section. The risk of failure for individual stent struts and hinges was examined in Harewood and McHugh[16] using micro-mechanical, rate-dependent, crystal plasticity based models of individual stent struts and hinges. These models used an explicit representation of individual FCC grains in the 316L microstructure, shown in Fig. 4, and incorporated an explicit representation of material failure based on void growth, through a modified Rice and Tracey[23] criterion.

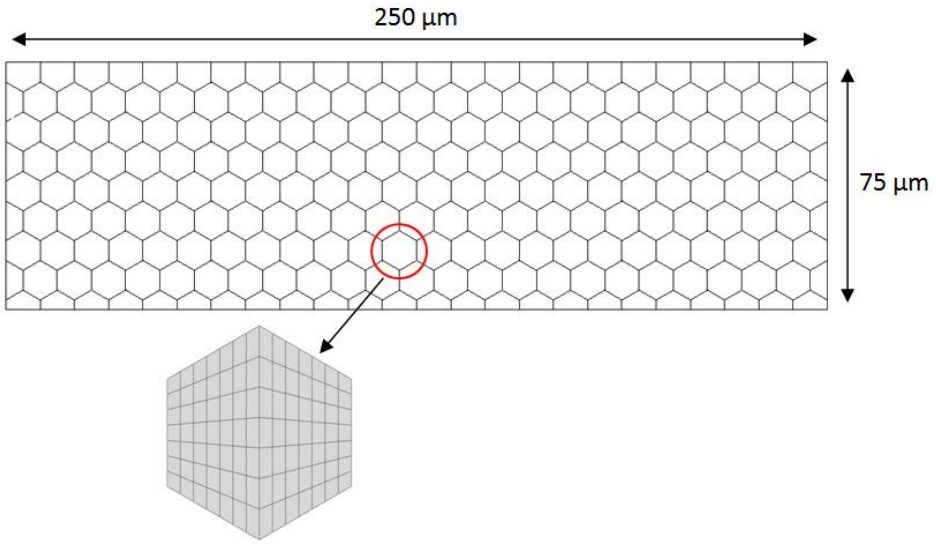

Fig. 4. Model of a 316L stainless steel strut with a thickness of 75 µm. The granular microstructure is idealized as a series of hexagons. A representation of the finite element mesh used is also shown for a single grain.

The failure of thin stainless steel struts in uni-axial tension was simulated, an example of which is shown in Fig. 5. From such simluations a relationship between strut thickness and overall strain at failure was derived. In addition to this, failure of struts subject to pure bending was simulated, as shown in Fig. 6. This allowed for the determination of a relationship between strut thickness and overall curvature change at failure in bending. Similar relationships were derived for plastic hinges in straightening (unbending) and combined tension and bending. Harewood and McHugh[16] compiled their findings in a series of *safe design charts*, which are used in subsequent sections in this work to determine the likelihood of stent failure based on the local deformation of individual struts and hinges.

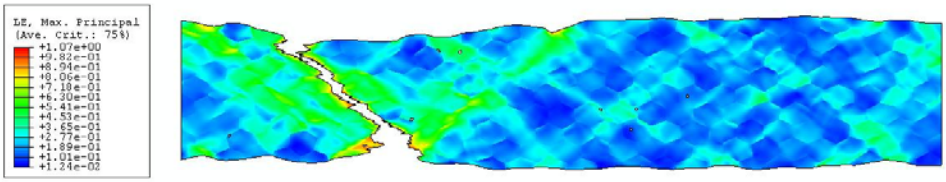

Fig. 5. Max principle logarithmic strains in a 75 µm thick strut that has failed in uni-axial tension.

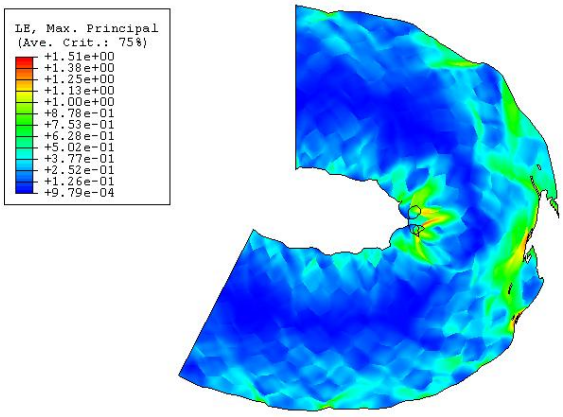

Fig. 6. Max principle logarithmic strains in a 75 μm thick strut that has failed under pure bending.

3. Deployment Simulations

Macroscale simulations of three common clinical stent deployment procedures are carried out in this study. However, a deployment in an idealized cylindrical artery is first performed to act as a baseline, allowing comparisons with subsequent simulations in more complex arterial geometries. In this initial analysis, the artery wall is modelled as a thin-walled cylinder and is meshed using 33 000 linear shell elements (S4R). The thickness of the wall is 0.55 mm, a commonly quoted thickness for the artery wall,[24] while its inner diameter is 3.75 mm. A further layer of 97 000 solid linear brick elements (C3D8R) is added to the external surface of the wall, so that physiologically realistic boundary conditions can be applied. This external layer is assigned a negligible elastic stiffness of $E = 0.01$ MPa, $\upsilon = 0.45$.

The nodes along the outer surface of this external layer are constrained in all degrees of freedom, allowing quite a free range of movement of the artery during stent deployment. This is considered a superior method of applying boundary conditions to the more common approach of artery tethering, as axial shortening of the artery is allowed. One end of the stent is constrained to motion in the radial direction only, allowing for a natural radial expansion of the stent. The stent, which is positioned to be concentric in the artery lumen, is deployed through the application of an internal pressure of 1.2 MPa, with an additional pressure of 0.8 MPa at its ends to ensure a realistic dog-bone profile.[18,19] A frictionless, hard contact is defined between the stent and artery wall. The ABAQUS®/Explicit finite element solver is used in this analysis with a typical solution time of 2.5 days on 4 processors of an SGI Altix 3700 high performance computer. It is found that failure of the stent is unlikely in this initial analysis, with the maximum curvature change in the most deformed plastic hinge being 4.7 rad/mm. It will be shown in subsequent analyses that there is little risk of failure for such a low curvature change.

3.1. *Deployment in a tortuous artery*

Stent deployment in a realistic tortuous artery geometry is now simulated. The artery geometry is taken from a healthy Right Coronary Artery (RCA) with an average internal diameter of 3.75 mm.[10] The artery wall is meshed using 90 000 linear shell elements

(S4R) with an outer layer of 270 000 linear brick elements (C3D8R). The nodes on the external surface of the outer layer are constrained in a similar manner to the previous analysis, with the same hard contact interaction defined between the stent and artery wall. The stent is initially deformed to conform to the curvature of the artery, as described in Sec. 2.1, and one end is constrained to allow only radial expansion prior to deployment. The stent is expanded with the same deployment pressures as used in the previous analysis. This analysis is performed using the ABAQUS®/Explicit finite element solver, with a typical solution time of approximately 2.5 days when solved using 6 processors on an SGI Altix 3700 high performance computer.

The progressive expansion of the stent can be seen in Fig. 7. During deployment the stent initially conforms to the artery walls. This results in good contact occurring on the lower surface of the lumen, but not on the upper surface. It is observed that maximum principal stresses and resulting deformations in the deployed stent in the curved artery are only slightly higher than those occurring in deployment in the straight artery. Failure in terms of strut fracture is thus deemed to be no more likely in deployment in curved arteries than in straight arteries. However, it is noted that if a stent were deployed with excessive compression on one side, that self contact between struts may occur. This has been experimentally observed to result in buckling of the stent lumen.[25] Since self contact is not observed between the struts in this analysis, failure of the device is not considered high risk.

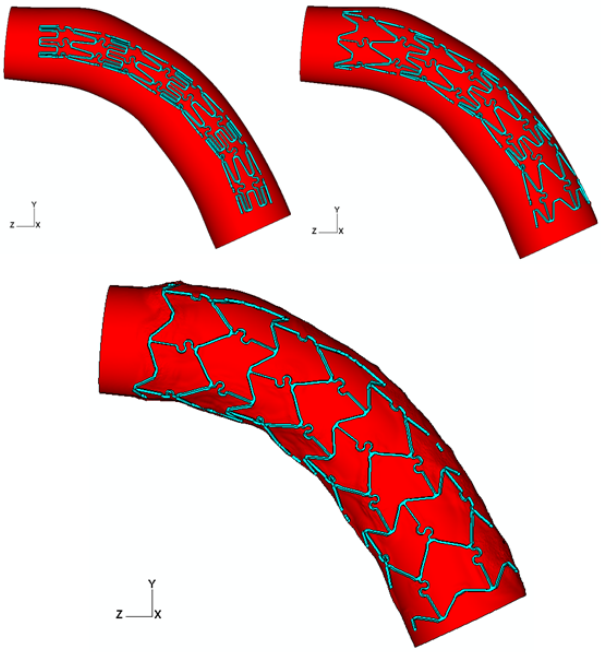

Fig. 7. Progressive stent expansion in the RCA to a final internal pressure of 1.2 MPa at the central section.

Although failure of the stent in deployment in the tortuous artery is deemed unlikely, it is noted in the course of this analysis that the magnitudes of maximum principal stresses in the artery wall, shown in Fig. 8(b), are three times higher than those observed

in the straight wall, shown in Fig. 8(a). This implies that the artery wall is subject to a far greater degree of deformation when tortuous arteries are being stented, potentially leading to an increased risk of patient injury through the onset of neointimal hyperplasia.[26]

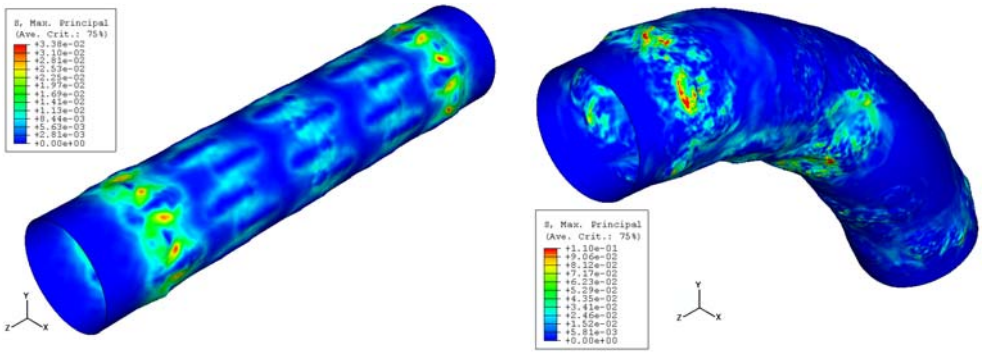

(a) (b)

Fig. 8. Plot of maximum principal stresses in the (a) Idealized straight artery (b) Realistic curved artery geometry. Units are in MPa. Significantly higher stresses are noted in the curved artery wall.

3.2. *'Burst out' deployment in a bifurcated artery*

In this analysis a stent deployment using the 'burst out' technique is simulated in a bifurcated or branched artery. The geometry of the artery used is based on that of a healthy Left Anterior Descending (LAD) arterial tree,[10] with a maximum inner diameter of 3.4 mm in the main artery. The LAD model, shown in Fig. 9(a), consists of two bifurcations, with the portion simulated in this paper circled. The 'burst out' technique involves the deployment of a stent in the main artery and main branch of the bifurcation. This is followed by the further expansion, or opening out, of one cell of the deployed stent by the expansion of a second balloon, in order to allow for the insertion of a second stent in the side branch. The section of the bifurcated artery simulated in this analysis is shown in Fig. 9(b), with an average internal diameter of 2.8 mm in the main branch. The deployment of a second stent in the side branch is not modelled in this work, and as a result the majority of this branch is removed for computational efficiency. The artery wall is meshed using 184 000 linear triangular shell elements (S3R). A thick shell implementation is used to represent the artery wall in this model, replacing the use of the solid tetrahedral elements (C3D4) of the previous analysis. This is deemed necessary due to difficulties encountered when meshing the complex geometry of the LAD model and also in implementing contact interactions. One limitation of this approach is that the physiologically realistic boundary conditions employed in previous analysis cannot be implemented, with artery tethering or fixation of both ends of the artery, used in their place. This is deemed acceptable for this analysis however, as the length of the artery modelled is considerably greater than that of the stent.

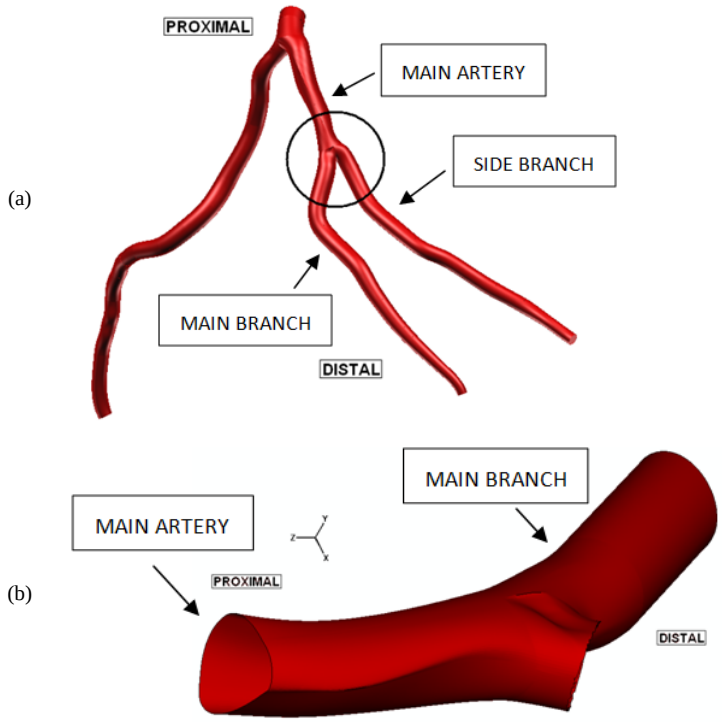

Fig. 9. Model of the LAD arterial tree. The bifurcation chosen for the simulations in this paper is circled. The main artery, main branch and side branch of this bifurcation are indicated. Proximal (rear) and distal (forward/leading) ends of the tree are also indicated; the terms proximal and distal are indentified through the direction of blood flow: proximal to distal. (b) The portion of the artery bifurcation used in the simulation of the 'burst out' procedure. The majority of the side branch is removed for computational efficiency.

In modelling the 'burst-out' procedure herein, deployment proceeds under an inflation pressure of 1.2 MPa and an additional pressure of 0.9 MPa at the ends. Following the deployment step, an additional step is modelled in which a uniform pressure of 4 MPa is applied normal to the highlighted surface in Fig. 10, to achieve further expansion of the cell located at the entrance to the side branch. This method is used for practicality, given the size and complexity of the computational problem addressed. A frictionless, exponential pressure-overclosure relationship is defined between the outer surface of the stent and the artery. The clearance between the surfaces at which the contact pressure is zero, is 0.01mm, and the contact pressure at zero clearance is 400 MPa. This defines a softened contact relationship that does not generate the excessive mesh distortion that hard contact can. The analysis is performed using the ABAQUS®/Explicit finite element solver with a typical solution time of 10 days on 8 cores of a Bull NovaScale 6320 high performance computer. Fig. 11 shows the view from the proximal end of the main vessel before (a) and after (b) the 'burst out' procedure. It can be seen that a sufficient opening has been made in the side of the stent for the insertion of another stent in the side branch.

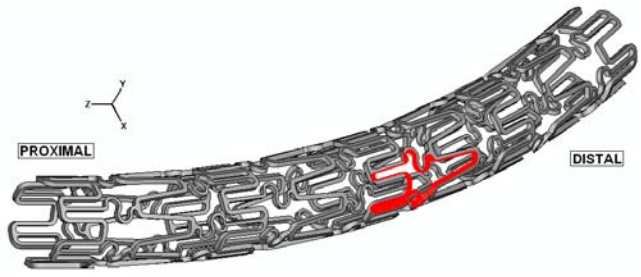

Fig. 10. Stent in position in main artery and main branch (artery not shown) before deployment. Proximal (rear) and distal (forward/leading) ends of stent indicated. Following deployment of the stent in the 'burst out' analysis, a pressure is applied to the highlighted surface to simulate the further opening out of this cell.

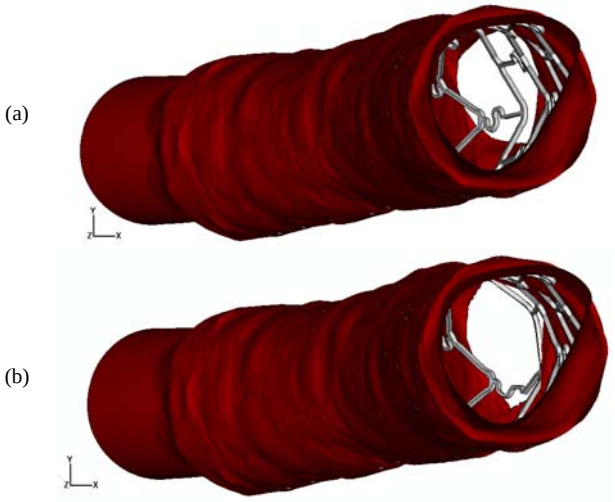

Fig. 11. View from the proximal end of the main vessel (a) prior to and (b) post 'burst out'. A clearance at the bifurcation can be seen after the 'burst out' procedure.

Stresses in the stent prior to the 'burst out' procedure are not high and fracture is deemed unlikely. However, during the 'burst out' procedure the hinges of the stent are subject to large plastic strains. It is important to assess the likelihood of failure of these plastic hinges and resulting failure of the stent. In the context of the overall failure risk assessment methodology presented herein, this is done through the use of the *safe design charts* developed by Harewood and McHugh,[16] which are based on the microscale modelling of failure in thin struts and plastic hinges described in Sec. 2.2. These charts, for example the one shown in Fig. 12(b) which is appropriate for the plastic hinges of interest in the stent geometry considered herein, are analogous to a Goodman diagram, with each curve delineating the boundary between safe performance and failure for a given strut thickness. Failure points for thin hinges due to strain in tension and curvature change in bending are plotted on the respective x- and y-axes for given thicknesses, with failure points in combined tension and bending populating the space between axes.

(a)

(b)

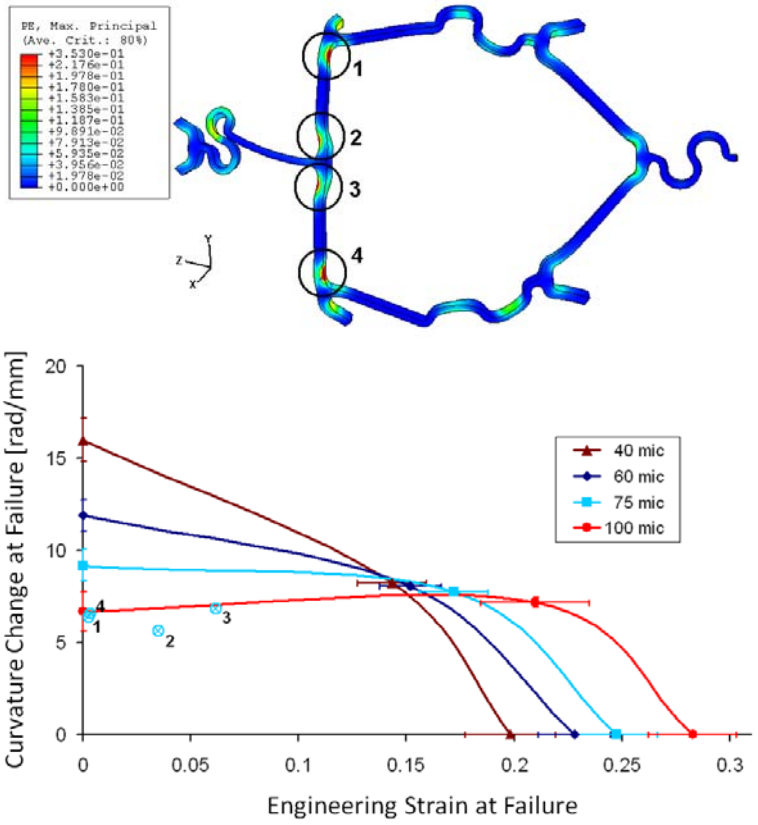

Fig. 12. (a) Plot of max principal plastic strain in the region of the stent deformed during the 'burst out' procedure. Numbered regions correspond to the hinges at which strains are highest. (b) Safe design chart for a plastic hinge from Harewood and McHugh[16] that is appropriate for the plastic hinges of interest here. The chart identifies safe and unsafe regions, on axes of curvature change vs. engineering strain, for hinges of different indicated thicknesses. Points corresponding to curvature changes and strains in hinges 1-4 are included for hinges of 75 μm thickness.

There are four regions (hinges) of the expanded cell that are significantly deformed, numbered 1-4 in Fig. 12(a). The measures of curvature change and engineering strain for each hinge are correspondingly plotted in Fig. 12(b). The engineering strain for each hinge is determined by identifying the initial length of a midline along the hinge, calculating the change in length of the midline as a result of the deformation, and dividing this change by the initial length. The curvature change is determined by measuring the change in angle subtended by the ends of the hinge (the cross-sections at each end of its initial length) during deformation and dividing by the length of the hinge, taking account of any the length change that might occur during deformation. As can be clearly seen from Fig. 12(b), all four data points fall within the safe performance region for a 75 μm strut thickness. The curvature change in each of the hinges is similar at approximately 6 rad/mm. However, the plastic hinges at the top and bottom of the expanded cell, numbered 1 and 4, are not subjected to tension, meaning the engineering

strain is negligible. The effect of the strain experienced by hinge numbers 2 and 3 increases the relative risk of failure (although still within the safe zone), especially for hinge 3, due to the influence of the nearby flexible link.

It is noted that in previous analyses of stent deployments in the straight and curved arteries that a curvature change of 4.7 rad/mm resulted in the most plastically strained hinges. Since these hinges were subject to negligible tensile strain, it can be seen from Fig. 12(b) that failure is unlikely in these hinges.

3.3. *'Crush' deployment in a bifurcated artery*

The 'crush' technique is the most commonly used multiple-stent bifurcation procedure.[27] It is designed to ensure complete coverage of the bifurcated region with stents, in order to provide full drug delivery from DES. In this procedure, stents are deployed in both branches of a bifurcation. A stent is initially deployed in the side branch, with its proximal end remaining in the main artery. A second balloon is then inflated in the main artery, crushing the portion of original stent that remains in the main artery and allowing the deployment of a second stent in the main branch. Since the deployment of the second stent is not modelled in this analysis, the majority of the main branch is removed for computational efficiency. The resulting section of the artery, as is simulated in this analysis, is shown in Fig. 13, with an average internal diameter of 2.6 mm. The artery wall is meshed using 397 000 linear triangular shell elements (S3R) with a thick walled implementation used for similar reasons to those described in the simulation of the 'burst out' technique.

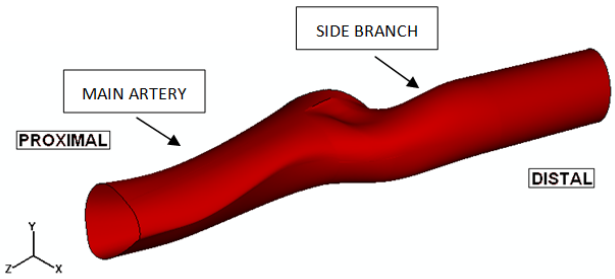

Fig. 13. The portion of the bifurcated artery used in simulating the 'crush' procedure. The majority of the main branch has been removed for computational efficiency.

In simulating this procedure herein, the stent is deployed in the side branch with a deployment pressure of 1.2 MPa and an additional pressure of 0.9 MPa at its ends. In order to simulate the crushing of the stent by the balloon, a distributed load of 3.5 MPa is applied in the positive X-direction on the highlighted face at the proximal end of the stent in Fig. 14. During the deployment step the boundary conditions are applied in the same manner as used in the 'burst out' analysis. However, during the crushing step each node in the artery mesh is fully constrained. This is a practical necessity to overcome the dynamic oscillation problems associated with the explicit finite element solution method, which are well documented in the literature.[28,29] The exponential pressure-overclosure contact relationship of the 'burst out' analysis is once again used in this analysis.

However self-contact is also defined for the stent, as it is more likely that stent struts will come into contact in this analysis. This increases the solution time for this analysis somewhat, but results in a more faithful representation of the overall distortion.

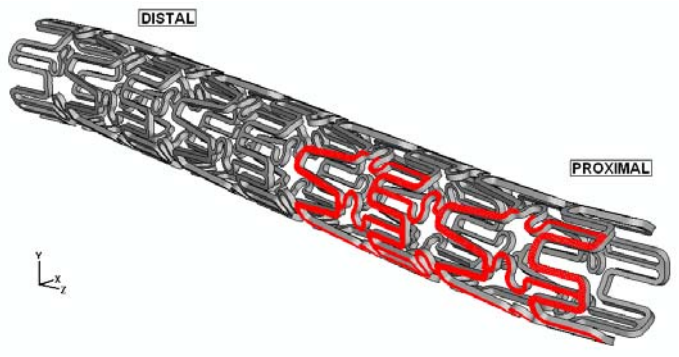

Fig. 14. Stent in position in main artery and side branch (artery not shown) before deployment. Following deployment, a pressure is applied to highlighted surface at the proximal end to crush the stent.

A typical solution time with ABAQUS®/Explicit is 13 days on 8 cores of an SGI Altix 3700 high performance computer. Following the crushing of the stent, access to the main branch is restored. A view from the proximal end of the stent in Fig. 15 shows that the procedure would be deemed a success from a clinical perspective; however considerable strut distortion is also seen to have taken place.

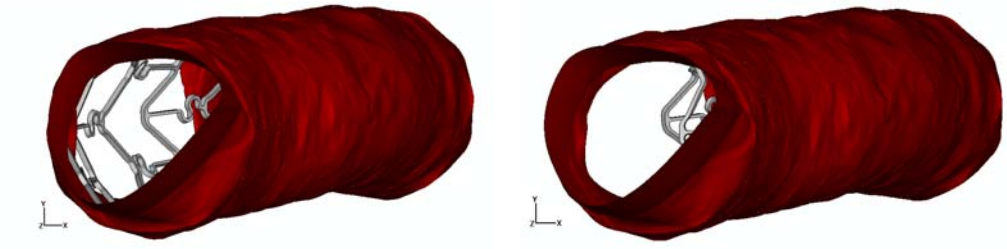

(a) (b)

Fig. 15. View from the proximal end of the main vessel illustrating the accessibility into the main branch (a) following initial stent deployment, and (b) following crushing of the stent.

There are numerous sites that experience large plastic strains in this analysis. The most obvious sites experiencing the most significant deformation are selected and shown in Fig. 16(a). The curvature changes and engineering strains in the hinges numbered 5 and 6 are determined, in the same manner as described in the analysis of Sec. 3.2 and the results are plotted on the same *safe design chart* from Harewood and McHugh.[16] It can be seen from Fig. 16(b) that these hinges are all in the safe performance region, but relatively speaking failure of these hinges is a greater risk than for those of the 'burst out' analysis. This can be attributed to the influence of the nearby flexible link, which connects these hinges to the distal end of the stent. This link is seen to transmit an additional tensile load to the hinge during crushing, resulting in an additional tensile strain.

(a)

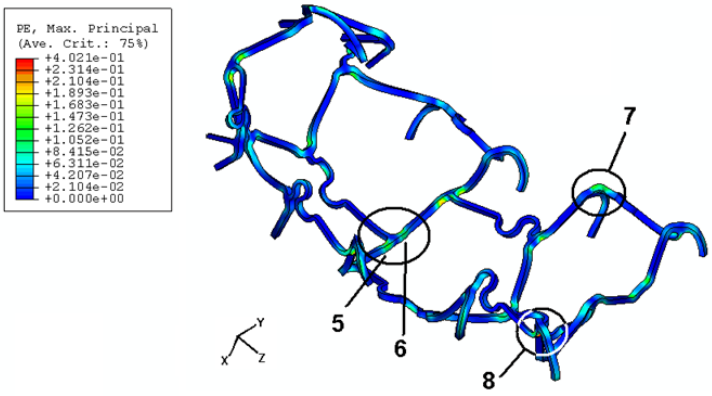

(b)

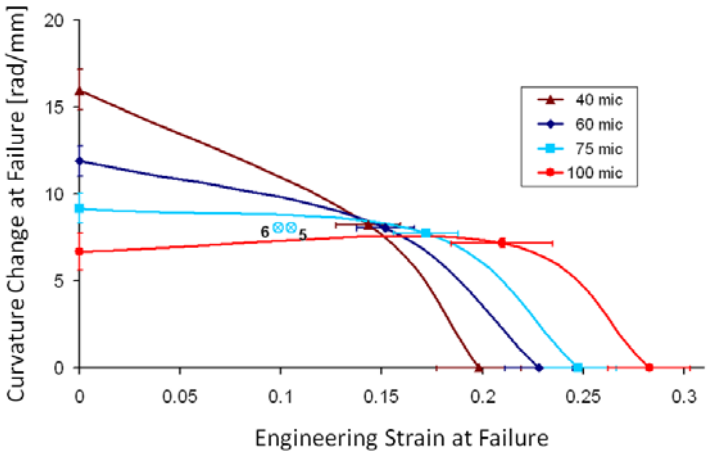

Fig. 16. (a) Plot of the max principal plastic strain profile in the crushed region of the stent. The majority of the stent has been removed for clarity. The regions of the stent that are investigated are ringed. (b) Safe design chart for a plastic hinge from Harewood and McHugh,[16] that is appropriate for the plastic hinges of interest here. The chart identifies safe and unsafe regions, on axes of curvature change vs. engineering strain, for hinges of different indicated thickness. The curvature changes and strains of the plastic hinges numbered 5 and 6 are plotted for hinges of 75 μm thickness.

The other two sites of the stent that are investigated are not plastic hinges. Strut number 7 is part of an 'S' bend in a flexible link that is connected to a plastic hinge. It is an initially curved strut that becomes more curved when the stent is crushed. Strut number 8 is initially a straight strut that bends during crushing. Due to the fact that the struts are not plastic hinges, the deformation measures must be plotted on a more general *safe design chart*. This is based on the microscale simulation of the loading of straight struts in tension and pure bending by Harewood and McHugh.[16] This chart, shown in Fig. 17, operates in a similar manner to the *safe design chart* shown in Fig. 16, with engineering strains and curvature changes for the various struts in the macroscale model calculated in a similar fashion to that described above for the hinges.

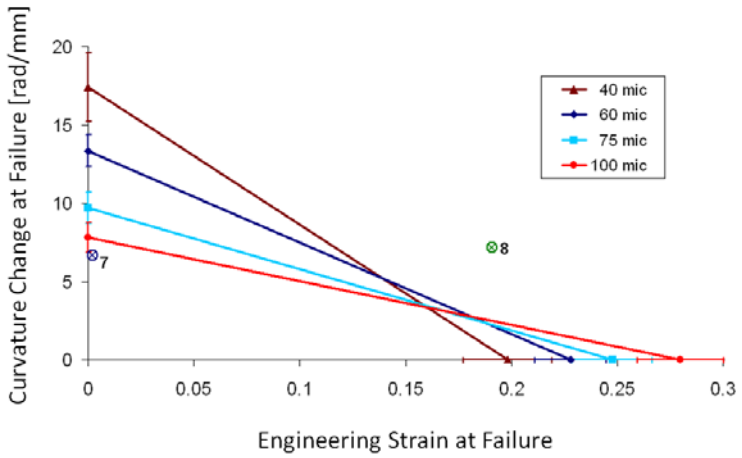

Fig. 17. Safe design chart for a straight strut from Harewood and McHugh,[16] that is appropriate for the struts of interest here. The chart identifies safe and unsafe regions, on axes of curvature change vs. engineering strain, for struts of different indicated thicknesses. The curvature changes and strains of struts 7 and 8 are plotted for struts of 75 μm thickness.

It can be seen from Fig. 17 that the flexible link, numbered 7, is in the safe performance region. However, the loading of the straight strut, numbered 8, is the most severe of either of the bifurcation analyses considered here. The results indicate that strut number 8 lies outside the safe performance region, indicating a potential risk of failure. In the event of strut fracture, the broken strut could damage the artery wall and possibly pierce it. Indeed, clinical findings have shown that strut fracture causes increased incidence of restenosis,[3] with detection of the fracture likely to prove difficult.

4. Discussion and Conclusions

The use of a multiscale approach in the modelling of stent deployment has allowed for the development of a size-dependent assessment methodology for strut failure risk. The methodology has been illustrated through the consideration of stenting procedures in straight, tortuous and bifurcated arteries.

It has been shown that for the particular bifurcated artery treatments considered here, significant deformation and distortion of the stent occurs, that is considerably more than for the straight and tortuous artery cases examined. For the generic stent geometry considered, the ‘crush’ technique generates the most severe distortion, with the methodology suggesting one instance of a risk of strut failure for the particular deployment conditions simulated. The fundamental reason for the failure risk indication in this case is that the stent has been severely distorted, as part of the ‘crush’ technique, in a fashion that is highly unconventional and irregular, relative to the uniform radial and circumferential expansion normally assumed as part of the conventional stent design process. In the ‘crush’ simulation, the region with the risk of failure is a straight strut that was not designed for bending, but that is bent and stretched during the distortion of the stent. This contrasts with the situation for the straight and tortuous arteries, where deformation of the stent in deployment is confined largely to the plastic hinges. This means that only regions that were designed to undergo bending in deployment do so.

In relation to the artery itself, it is of interest to note the significantly higher stresses experienced in the wall of the tortuous artery during stenting, in comparison to the straight artery. Despite the safety of the stent itself in these cases, it is far more likely that injury to the artery wall could occur in the curved artery in comparison to the straight one. This has further implications in terms of restenosis, as it has been found that neointimal hyperplasia can be related to localized arterial damage from stent struts impinging on artery walls.[26]

In overall terms, the authors believe that the size-dependent stent deployment failure risk assessment methodology presented here is valuable, and of potential direct use as part of the stent design process. The implementation of the method as presented here does have its limitations, as discussed below. However, the principle of the multiscale modelling method, as illustrated by the specific cases considered herein, does, at the very least, allow for an indication to be obtained on instances where unacceptable levels of deformation (implying a risk of failure) may be occurring for a given stent design in a given deployment configuration. This then can point the way for further detailed analysis, design modifications and prototype testing to optimize the geometrical design of the stent.

As regards the implementation of the methodology presented here, there are limitations. The accuracy of the macroscale modelling is limited by a number of simplifying assumptions. These assumptions, detailed in the previous sections, are practically necessary to successfully perform the simulations, and are the result of the significant geometrical complexity and the very large numerical problem sizes (which even with the simplifying assumptions took on the order of weeks on parallel high performance computers). Chief amongst the assumptions is the deployment action using surface pressure and not an explicit representation of the balloon, as in Refs 9, 20 and 21, which would have been preferable, and which would have provided a superior way of dealing with the simulation of the dog-boning effect and the 'burst out' loading for example. However the inclusion of an explicit balloon representation would have made the current problem complexity impractical, as has been suggested by Stolpmann *et al.*[30] Additionally, the basis for the development of the failure risk assessment method depends on the final deformed configuration of the stent; the details of the history of the expansion process itself, assuming that it is reasonably monotonic, are of secondary importance. Having said this though, it is likely that in the tortuous artery and bifurcation artery simulations actual balloon expansion (and hence an explicit representation in the models) would have led to an increased straightening of the stent in the curved geometries, relative to what is achieved here using uniform internal pressure. It is unlikely that this would lead to an increased deformation in the stent struts, however higher stresses in the artery wall than those predicted in this work might have resulted.

From the microscale modelling point of view, to generate a data base of safe design charts that would be useful in practice, the microscale simulations described above (as performed in Harewood and McHugh[16] for a range of strut thicknesses) would need to be repeated for a wide range of hinge radii and material microstructures (i.e. average grain sizes). Going further, such simulations would need to be performed (and experimentally validated) for newly emerging stent materials such as cobalt-chromium alloys. The latter is the topic of current work by the authors.

Acknowledgements

The authors would like to acknowledge funding from the Irish Research Council for Science, Engineering and Technology, under the EMBARK program (F. Harewood and J. Grogan), funded by the National Development Plan, and the SFI/HEA Irish Centre for High-End Computing (ICHEC) for the provision of computational facilities and support. The simulations in this work were performed on the SGI Altix 3700 high performance computer at NUI Galway and the Bull NovaScale 6320 at ICHEC. Dr. L. O'Keeffe and Prof. T. McGloughlin are acknowledged for the provision of realistic arterial geometries.

References

1. J. Mackay, G. A. Mensah, S. Mendis, K. Greenlund and W. H. Organization, *The atlas of heart disease and stroke,* (World Health Organization, 2004).
2. B. L. van der Hoeven, N. M. M. Pires, H. M. Warda, P. V. Oemrawsingh, B. J. M. van Vlijmen, P. H. A. Quax, M. J. Schalij, E. E van der Wall and J. W. Jukema, Drug-eluting stents: results, promises and problems, *Int. J. Cardiol*. **99** (2005) 9-17.
3. G. Sianos, S. Hofma, J. M. R. Ligthart, F. Saia, A. Hoye, P. A. Lemos and P. W. Serruys, Stent fracture and restenosis in the drug-eluting stent era, *Catheter. Cardiovasc. Interv*. **61** (2004) 111-116.
4. H. Takebayashi, G. S. Mintz, S. G. Carlier, Y. Kobayashi, K. Fujii, T. Yasuda, R. A. Costa, I. Moussa, G. D. Dangas, R. Mehran, A. J. Lansky, E. Kreps, M. B. Collins, A. Colombo, G. W. Stone, M. B. Leon and J. W. Moses, Nonuniform strut distribution correlates with more neointimal hyperplasia after sirolimus-eluting stent implantation, *Circulation,* **110** (2004) 3430-3434.
5. F. Etave, G. Finet, M. Boivin, J. Boyer, G. Rioufol and G. Thollet, Mechanical properties of coronary stents determined by using finite element analysis, *J. Biomech*. **34** (2001) 1065-1075.
6. C. Dumoulin and B. Cochelin, Mechanical behaviour modelling of balloon-expandable stents, *J. Biomech*. **33 (**2000) 1461-1470.
7. C. Lally, F. Dolan and P. Prendergast, Cardiovascular stent design and vessel stresses: a finite element analysis, *J. Biomech*. **38** (2005) 1574-1581.
8. W. Walke, Z. Paszenda and J. Filipiak, Experimental and numerical biomechanical analysis of vascular stent, *J. Mater. Process. Tech*. **164-165** (2005) 1263-1268.
9. P. Mortier, M. De Beule, D. Van Loo, B. Verhegghe and P. Verdonck, Finite element analysis of side branch access during bifurcation stenting, *Med. Eng. Phys*. **31** (2009) 434-440.
10. L. O'Keeffe, T. O'Brien and T. McGloughlin, Method for Applying Realistic Coronary Wall Shear Stresses to in vitro Endothelial Cell Cultures, *Proc. 14th Conference European Society of Biomechanics*, Hertogenbosch, The Netherlands (2004).
11. B. P. Murphy, P. Savage, P. E. McHugh and D. F. Quinn, The Stress–Strain Behavior of Coronary Stent Struts is Size Dependent, *Ann. Biomed. Eng*. **31** (2003) 686-691.
12. B. Murphy, H. Cuddy, F. Harewood, T. Connolley and P. McHugh, The influence of grain size on the ductility of micro-scale stainless steel stent struts, *J. Mat. Sci. Mater. Med*. **17** (2006) 1-6.
13. F. Auricchio, M. D. Loreto and E. Sacco, Finite-element Analysis of a Stenotic Artery Revascularization Through a Stent Insertion, *Comput. Meth. Biomech. Biomed. Eng*. **4** (2001) 249-263.
14. S. N. D. Chua, B. J. Mac Donald and M. S. J. Hashmi, Finite element simulation of stent and balloon interaction, *J. Mater. Process. Tech*. **143-144** (2003) 591-597.
15. P. Savage, B. P. O' Donnell, P. E. McHugh, B. P. Murphy and D. F. Quinn, Coronary Stent Strut Size Dependent Stress–Strain Response Investigated Using Micromechanical Finite Element Models, *Ann. Biomed. Eng*. **32** (2004) 202-211.

16. F. J. Harewood and P. E. McHugh, Modeling of Size Dependent Failure in Cardiovascular Stent Struts under Tension and Bending, *Ann. Biomed. Eng*. **35** (2007) 1539-1553.
17. Hibbitt, Karlsson, and Sorenson, *ABAQUS Theory Manual*, Pawtucket, RI, USA (1997).
18. F. Migliavacca, L. Petrini, V. Montanari, I. Quagliana, F. Auricchio and G. Dubini, A predictive study of the mechanical behaviour of coronary stents by computer modelling, *Med. Eng. Phys*. **27** (2005) 13-18.
19. F. J. Harewood, *Micro and macromechanical modelling of cardiovascular stents in realistic arterial geometries*, PhD Thesis, NUI Galway, Galway, Ireland (2006).
20. P. Mortier, M. De Beule, S.G. Carlier, R. Van Impe, B. Verhegghe and P. Verdonck, Numerical study of the uniformity of balloon-expandable stent deployment, *J. Biomech. Engin*. **130** (2008) 021018-1.
21. F. Gervaso, C. Capelli, L. Petrini, S. Lattanzio, L. Di Virgilio and F. Migliavacca, On the effects of different strategies in modelling balloon-expandable stenting by means of finite element method, *J. Biomech*. **41** (2008) 1206-1212.
22. P. J. Prendergast, C. Lally, S. Daly, A. J. Reid, T. C. Lee, D. Quinn and F. Dolan, Analysis of prolapse in cardiovascular stents: a constitutive equation for vascular tissue and finite-element modelling, *J Biomech. Eng*. **125** (2003) 692-699.
23. J. R. Rice and D. M. Tracey, On the ductile enlargement of voids in triaxial stress fields, *J. Mech. Phys. Solids*, **17** (1969) 201-217.
24. I. Ozolanta, G. Tetere, B. Purinya and V. Kasyanov, Changes in the mechanical properties, biochemical contents and wall structure of the human coronary arteries with age and sex, *Med. Eng. Phys*. **20** (1998) 523-533.
25. K. Mori and T. Saito, Effects of Stent Structure on Stent Flexibility Measurements, *Ann. Biomed. Eng*. **33** (2005) 733-742.
26. J. M. Garasic, E. R. Edelman, J. C. Squire, P. Seifert, M. S. Williams and C. Rogers, Stent and artery geometry determine intimal thickening independent of arterial injury, *Circulation*, **101** (2000) 812-818.
27. A. Colombo and T. Lefevre, Bifurcational Stenting, *Proc. 54th Annual Scientific Session of the American College of Cardiology*, Orlando, Florida, USA (2005).
28. H. Choi, S. Hwang, Y. Kang, J. Kim and B. Kang, Comparison of Implicit and Explicit Finite-Element Methods for the Hydroforming Process of an Automobile Lower Arm, *Intl. J. Adv. Manufac. Tech*. **20** (2002) 407-413.
29. L. M. Kutt, A. B. Pifko, J. A. Nardiello and J. M. Papazian, Slow-dynamic finite element simulation of manufacturing processes, *Comput. Struct*. **66** (1998) 1-17.
30. J. Stolpmann, H. Brauer, H. Stracke, R. Erbel and A. Fischer, Practicability and Limitations of Finite Element Simulation of the Dilation Behaviour of Coronary Stents, *Materialwissenschaft und Werkstofftechnik*, **34** (2003) 736-745.